

Article

## Thermal Balance Analysis of a Micro-Thermoelectric Gas Sensor Using Catalytic Combustion of Hydrogen

Daisuke Nagai, Takafumi Akamatsu, Toshio Itoh, Noriya Izu and Woosuck Shin \*

AIST, 2266-98 Anagahora, Shimo-Shidami, Moriyama-ku, Nagoya 463-8560, Japan;  
E-Mails: d-nagai@aist.go.jp (D.N.); t-akamatsu@aist.go.jp (T.A.); itoh-toshio@aist.go.jp (T.I.);  
n-izu@aist.go.jp (N.I.)

\* Author to whom correspondence should be addressed; E-Mail: w.shin@aist.go.jp;  
Tel.: +81-52-736-7107; Fax: +81-52-736-7244.

Received: 16 December 2013; in revised form: 13 January 2014 / Accepted: 14 January 2014 /  
Published: 21 January 2014

---

**Abstract:** A thermoelectric gas sensor (TGS) with a combustion catalyst is a calorimetric sensor that changes the small heat of catalytic combustion into a signal voltage. We analyzed the thermal balance of a TGS to quantitatively estimate the sensor parameters. The voltage signal of a TGS was simulated, and the heat balance was calculated at two sections across the thermoelectric film of a TGS. The thermal resistances in the two sections were estimated from the thermal time constants of the experimental signal curves of the TGS. The catalytic combustion heat  $Q_{catalyst}$  required for 1 mV of  $\Delta V_{gas}$  was calculated to be 46.1  $\mu$ W. Using these parameters, we find from simulations for the device performance that the expected  $Q_{catalyst}$  for 200 and 1,000 ppm H<sub>2</sub> was 3.69  $\mu$ W and 11.7  $\mu$ W, respectively.

**Keywords:** thermoelectric gas sensor; combustion catalyst; thermal balance

---

### Nomenclature

$P$	heating power input
$T$	temperature
$t$	time
$R$	thermal resistance
$Q_{catalyst}$	heat generation of catalytic combustion

$Q_{heaterA}$	heat generation of heater for section A
$Q_{heaterB}$	heat generation of heater for section B
$T_{ambient}$	ambient temperature, mainly room temperature
$\Delta T_{AB}$	temperature difference between sections A and B
$T_A$	temperature in section A
$T_B$	temperature in section B
$C_A$	heat capacity of section A
$C_B$	heat capacity of section B
$R_A$	thermal resistance of section A
$R_B$	thermal resistance of section B
$V_S$	voltage signal of the TGS
$V_{gas}$	voltage signal in the combustion gas
$V_{air}$	voltage signal in air
$\Delta V_{gas}$	voltage difference between the responses in air and the inflammable gas
$\tau_A$	thermal time constant of section A
$\tau_B$	thermal time constant of section B

## 1. Introduction

Inflammable gases such as CO, CH<sub>4</sub>, and H<sub>2</sub>, which can amount to several hundred parts per million in human breath [1,2], can be used for medical examination and detected by the micro-calorimetric device of a thermoelectric gas sensor (TGS) with a combustion catalyst. The TGS can be a useful platform device, because it is possible to modify the catalyst of the TGS for the target gas. We have reported that a TGS with a Pt-loaded alumina (40 wt%Pt/alumina) catalyst can detect H<sub>2</sub> over a wide concentration range from as low as 0.5 ppm up to 5 vol.% H<sub>2</sub> in air [3]. In addition, this device showed a good linearity between the H<sub>2</sub> concentration in air and the sensing signal at the catalyst temperature of 100 °C. We have succeeded in measuring H<sub>2</sub> in the human breath at the parts per million level [4]. Additional improvements in the TGS device are required for the detection of CO and CH<sub>4</sub>, such as much higher catalyst temperature and precise temperature control, because CO and CH<sub>4</sub> are less inflammable as compared to H<sub>2</sub>. The thermal design of a TGS should be improved for efficient transport of the catalytic combustion heat of CO and CH<sub>4</sub>. In order to produce an effective design, the heat balance of the sensor during operation needs to be estimated. Moreover, the heat balance can predict the inflammable gas combustion energy of the catalyst, as the heat as a function of the sensor output is also important for the development of the catalyst. However, the heat of combustion of the small amount catalyst which is used for gas sensors is difficult to estimate since it is difficult to measure the temperature of small parts of devices like sensors.

In this paper, a calculation for the heat balance of both ends of the thermoelectric (TE) film of a sensor device is presented, and the sensor output is simulated. Calculations for the rate of catalytic combustion converted to a voltage signal using a heat balance calculation are compared with the experimental results that estimate the rate of catalytic combustion of a TE hydrogen sensor.

## 2. TGS Device Preparation

Figure 1 shows a photograph of the micro-TGS with the ceramic combustion catalyst used in this study. A double-sided polished Si substrate with a thickness of 0.35 mm was used. A silicon-germanium (SiGe) thin film was deposited by DC magnetron sputtering and patterned into the TE material by RIE etching. Micro-heater and electrode lines were fabricated using a lift-off technique involving platinum. To fabricate a membrane structure, the bottom of the substrate was etched using an aqueous KOH solution. The detailed process has been previously reported [5]. A metal colloid solution was stirred constantly, followed by the addition of  $\text{Al}_2\text{O}_3$  powder to the solution to create a catalyst powder of 40 wt% metal content. Then, distilled water was added to the solution, and the solution was agitated at 70 °C until the water evaporated. The solid residue obtained was dried at 90 °C for 30 min and then baked in air at 300 °C for 2 h to obtain the catalyst powder. A ceramic paste of the catalyst was prepared by mixing terpeneol, ethyl cellulose, and distilled water at a weight ratio of 9:1:5. A drop of the ceramic paste was placed on the thin membrane of the micro-TGS using an air dispenser. The size of the drop on the membrane could be controlled to 0.6 mm in diameter by changing the dispensing time and air pressure. After paste deposition, the device was baked in air at 300 °C for 2 h.

**Figure 1.** Optical image of the TGS (on the stem). Cross-sectional view of the TGS on the stem. Two sections of the heater meander line on the membrane are called sections A and B, and the center section of straight heater line is called section C.

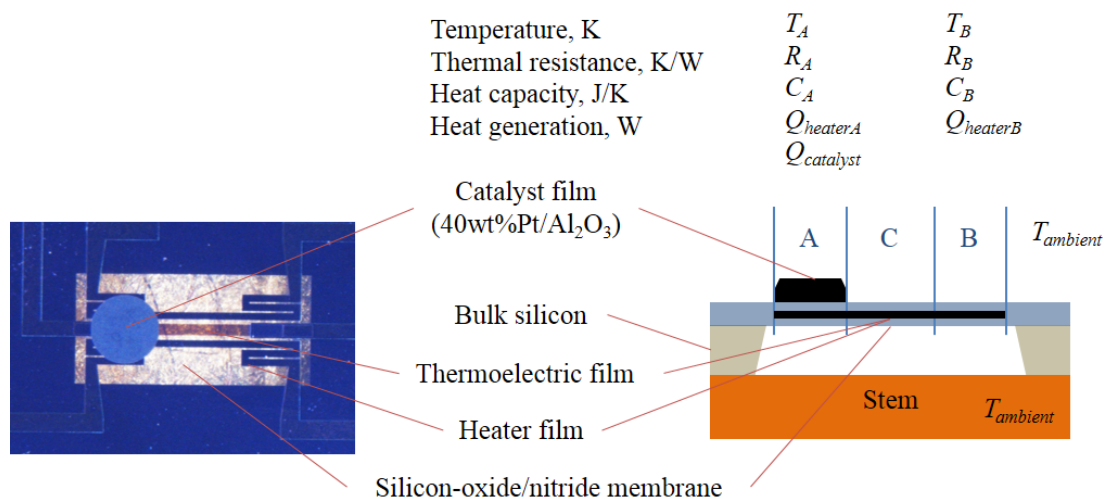


Table 1 lists the material constants and boundary conditions for the TGS used in this study. The heat capacity of the dispensed 40 wt%Pt/Al<sub>2</sub>O<sub>3</sub> catalyst,  $C_{catalyst}$ , was 4.34  $\mu\text{J/K}$ , as estimated from the specific heat capacity, density and volume. The catalytic specific heat capacity was estimated from the catalytic constituent and material constants for Pt and Al<sub>2</sub>O<sub>3</sub>. The dimensions of the dispensed catalyst, diameter, thickness, and volume were measured using a P16+ Profiler manufactured by KLA-Tencor. The heat capacities of the membrane,  $C_{membrane}$ , in sections A and B were assumed to be the same as  $C_{catalyst}$  since the size of the membrane and the size of the catalyst are similar.  $C_A$  was computed as the sum of  $C_{catalyst}$  and  $C_{membrane}$  and is equal to 8.68  $\mu\text{J/K}$ .  $C_B$  was simply equal to  $C_{membrane}$ , which is 4.34  $\mu\text{J/K}$ .  $\alpha$  was 0.2 mV/K in this study, as obtained from [3].

**Table 1.** Material constants and boundary conditions for the TGS used in this study.

Parameter	Symbol	Value	Unit	References
Specific heat capacity Pt	-	134	J/(kg K)	[6]
Density Pt	-	21.45	g/cm <sup>3</sup>	[7]
Specific heat capacity Al <sub>2</sub> O <sub>3</sub>	-	800	J/(kg K)	“Network database system for thermophysical property data” by AIST and 790 J/(kg K) is rounded to 800 J/(kg K).
Density Al <sub>2</sub> O <sub>3</sub>	-	4	g/cm <sup>3</sup>	Product data sheet by Taimei Chemicals Co., Ltd. and 3.95 g/cm <sup>3</sup> is rounded to 4.00 g/cm <sup>3</sup> .
Dispensed catalytic diameter	-	600	μm	Rounded from the values (565 and 4.64 μm) measured by a KLA-Tencor P16+ Profiler.
Dispensed catalytic thickness	$d_{catalyst}$	5	μm	
Dispensed catalytic volume	-	$1.41 \times 10^{-3}$	mm <sup>3</sup>	
Seebeck coefficient	$\alpha$	0.2	mV/K	Rounded from the measured value of 0.167 mV/K [3].
Heat capacity catalyst 40wt%Pt/Al <sub>2</sub> O <sub>3</sub>	$C_{catalyst}$	4.34	μJ/K	Estimated from the specific heat capacity and density for the catalyst.
Heat capacity for the membrane	$C_{membrane}$	4.34	μJ/K	The heat capacity of the membrane in sections A and B was assumed to be the same as the heat capacity of the catalyst.
Heat capacity for section A	$C_A$	8.68	μJ/K	$=C_{catalyst} + C_{membrane}$
Heat capacity for section B	$C_B$	4.34	μJ/K	$=C_{membrane}$
Ambient temperature	$T_{ambient}$	298	K	

The gas response of the sensor was investigated using a flow chamber. After placing a sensor in the flow chamber, air and the hydrogen were allowed to alternately flow into the chamber. The operating temperature was adjusted by heater control and the cold-side junction was monitored using an IR camera (Nikon, LAIRD-270A). The voltage signal from the sensor was monitored using a digital multimeter (KeithleyK2700).

### 3. Design and Detection Principle for the Calorimetric Device of a TGS

#### 3.1. Thermal Balance in a TGS

A TGS consists of a thermal sensor that detects the temperature difference. The heat balance for a thermal sensor is briefly denoted by the following equation [8–10]:

$$P = [T(t) - T_{ambient}] \times R^{-1} \quad (1)$$

The temperature difference  $T(t) - T_{ambient}$  depends linearly on the thermal resistance  $R$  and heating power input  $P$ . A sensor with a low heating power output and big thermal resistance leads to a large temperature difference. In the TGS, the hot and cold junctions of a TE film are on a membrane, which can reduce unwanted noise caused by air flow, for example. Therefore, the heat balances in two

junctions of a TE film become important and differ from each other in Equation (1). A TGS emits a signal  $V_S$  according to the temperature difference  $\Delta T$  between both ends of the TE film;  $\Delta T$  is determined by two energy balances of the TE film at both ends.

Figure 1 shows an optical image of the TGS device [3]. Two sections of the heater meander line on the membrane are called sections A and B, and the center section of the straight heater line is called section C. The two different temperatures at the heater meander sections A and B in the membrane are temperatures  $T_A$  and  $T_B$ , respectively, of the ends of the TE film in the lumped parameter system.  $V_S$  of the TGS can be expressed as follows from the Seebeck effect:

$$V_S = \alpha \times \Delta T_{AB} = \alpha \times (T_A - T_B) \quad (2)$$

where  $\alpha$  is the Seebeck coefficient of the TE film on the device. The influence of the temperature dependency of the Seebeck coefficient  $\alpha(T)$  can be neglected since the temperature shift is small in combusting low concentration gas. The heat balance of the hot section A and cold section B can then be expressed as follows. Two thermal energy balance equations are written as:

$$C_A \frac{dT_A(t)}{dt} = Q_{heater} + Q_{catalyst} - \frac{T_A(t) - T_{ambient}}{R_A} \quad (3)$$

$$C_B \frac{dT_B(t)}{dt} = Q_{heater} - \frac{T_B(t) - T_{ambient}}{R_B} \quad (4)$$

where  $C_A$  and  $C_B$  are the heat capacities of sections A and B, respectively;  $t$  is the time;  $Q_{heater}$  is the heat generation of the heater;  $T_{ambient}$  is the ambient temperature;  $Q_{catalyst}$  is the heat of the catalyst by inflammable gas combustion; and  $R_A$  and  $R_B$  are thermal resistances of conduction and convection to the ambient temperature of sections A and B, respectively.  $R_A$  and  $R_B$ —are constants since the gas flow velocity is constant.

### 3.2. Voltage Signal $\Delta V_{gas}$ for Inflammable Gas

The voltage signal  $\Delta V_S$  for combustion gas is the voltage difference between the saturated voltage of the TGS in inflammable gas  $V_{gas}$  and that in air  $V_{air}$ :

$$\Delta V_S = V_{gas} - V_{air} \quad (5)$$

When the TGS signal is saturated, the TGS is considered to be in a thermally steady state. Thus, the left-hand sides of Equations (3) and (4) can be set to zero at steady state ( $dT/dt = 0$ ), and be rewritten as follows:

$$T_A = R_A \times (Q_{heater} + Q_{catalyst}) + T_{ambient} \quad (6)$$

$$T_B = R_B \times Q_{heater} + T_{ambient} \quad (7)$$

To determine  $V_{gas}$ , Equations (6) and (7) are substituted into Equation (2):

$$V_{gas} = \alpha \times [R_A \times (Q_{catalyst} + Q_{heater}) - R_B \times Q_{heater}] \quad (8)$$

In order to solve for  $V_{air}$  as in Equation (8), Equations (6) and (7) are substituted into Equation (2), where  $Q_{catalyst}$  in Equation (6) is set to zero in air:

$$V_{air} = \alpha \times Q_{heater} \times (R_A - R_B) \quad (9)$$

In order to calculate  $\Delta V_{gas}$ , Equations (8) and (9) are substituted into Equation (5):

$$\Delta V_{gas} = \alpha \times Q_{catalyst} \times R_A \quad (10)$$

The parameters that determine  $\Delta V_{gas}$  for the TGS are  $\alpha$ ,  $Q_{catalyst}$ , and  $R_A$ .

### 3.3. Voltage Signal $V_S(t)$

If we consider that Equations (3) and (4) are a first-order system response, these equations can be changed into the following by Laplace analysis [8]:

$$T_A(t) - T_{ambient} = (Q_{heater} + Q_{catalyst}) \times R_A \times \left[ 1 - \exp\left(\frac{-t}{R_A \cdot C_A}\right) \right] \quad (11)$$

$$T_B(t) - T_{ambient} = Q_{heater} \times R_B \times \left[ 1 - \exp\left(\frac{-t}{R_B \cdot C_B}\right) \right] \quad (12)$$

Then, the thermal time constants  $\tau_A$  and  $\tau_B$  are expressed as follows:

$$\tau_A = R_A \times C_A \quad (13)$$

$$\tau_B = R_B \times C_B \quad (14)$$

If Equations (11) and (12) are substituted into Equation (2),  $V_S(t)$  is calculated as

$$V_S(t) = \alpha \times \left\{ (Q_{catalyst} + Q_{heater}) \times R_A \times \left[ 1 - \exp\left(\frac{-t}{R_A \times C_A}\right) \right] - Q_{heater} \times R_B \times \left[ 1 - \exp\left(\frac{-t}{R_B \times C_B}\right) \right] \right\} \quad (15)$$

The time constant of the voltage signal  $\tau_S$  in Equation (15) is determined by the correlation of sections A and B. Furthermore,  $\tau_S$  depends only on section A, indicating that  $\tau_S = \tau_A$  when the sensor is thermally stabilized by heating, and the combustion gas is introduced.

## 4. Experimental Verification and Discussions

### 4.1. Voltage Signal Response $V_S(t)$ of the TGS for Hydrogen Gas

The  $Q_{catalyst}$  is proportional to the hydrogen concentration of the air flow [3]. It is assumed that the catalyst combustion energy  $Q_{catalyst}$  is the constant in Equations (3) and (4). In TGS, the catalyst combustion energy is proportional to the gas concentration such as the  $H_2$ . It takes time that the gas concentration in the chamber reaches the gas concentration of the flow to the chamber when the certain gas concentration flows to the chamber. So, the catalyst combustion heat is not the ideal constant parameter since the gas concentration in the chamber is not constant.

**Figure 2.** Experimental response curve of the TGS for 200 ppm H<sub>2</sub> and the flow rate from 200 ccm to 1,800 ccm. The thermal time constant, measured as the elapsed time from 60 s to decreasing at 63.2% of the  $\Delta V_{gas}$ . The catalyst of the TGS device was heated up to 120 °C by its micro-heater. H<sub>2</sub> flow was from 30 to 60 s.

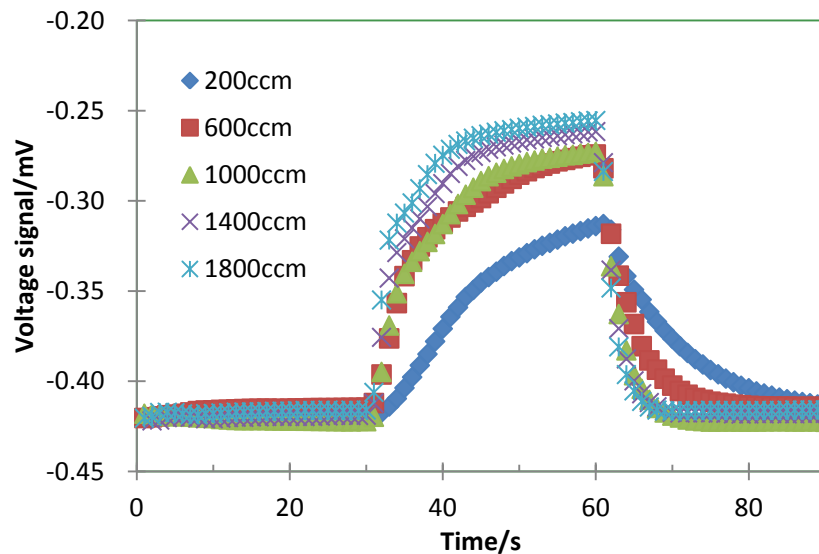


Figure 2 shows the voltage signal response curve of the TGS for 200 ppm H<sub>2</sub>. The catalyst of the TGS device was heated up to 120 °C by its micro-heater. First, air flowed up to 30 s, then H<sub>2</sub> flowed from 30 to 60 s, and then air flowed again, where the flow rate was changed from 200 to 1,800 ccm. The time constant is small by the gas mass flow because the time until the hydrogen concentration in the chamber reaches to 200 ppm is short.

#### 4.2. Combustion Reaction Limited $V_S(t)$ of the TGS at High Gas Flow End

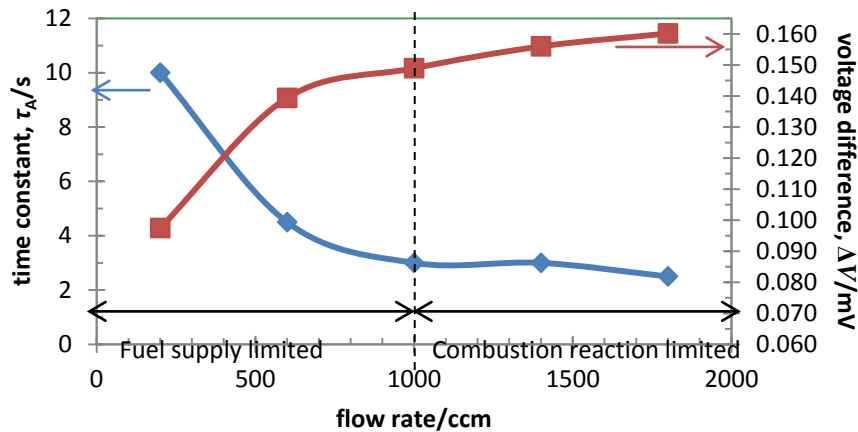
Figure 3 shows the flow rate dependence of the thermal time constant,  $\tau_A$ , and the voltage difference,  $\Delta V_{gas}$ , of the TGS for 200 ppm H<sub>2</sub> combustion under various gas flow rate from 200 to 1,800 ccm.  $\tau_A$  measured at the elapsed time from 60 s to decreasing at 63.2% of the saturated value of  $\Delta V_{gas}$ . For the gas flow rate below 1,000ccm,  $\tau_A$  decreased from 10 to 3 s with the flow rate, and became constant over 1,000 ccm.  $\tau_A$  will be independent of the flow rate in the reaction limited state.

In Figures 2 and 3,  $\Delta V_{gas}$  increased with the flow rate. If the operating temperature is high enough to activate the combustion, the reaction would be diffusion-limited, being controlled by the diffusion of the hydrogen gas to the catalyst surface.

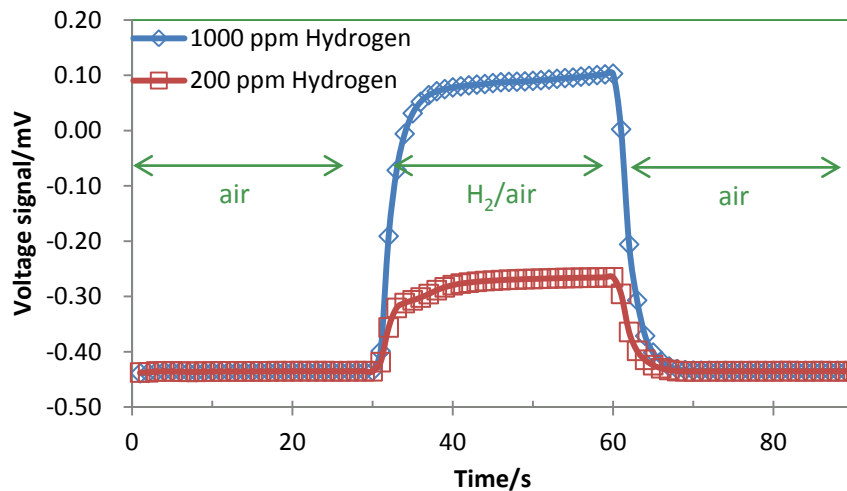
#### 4.3. Estimation of Thermal Time Constants

Figure 4 shows the response curves and  $\Delta V_{gas}$  of the TGS for 200 ppm and 1,000 ppm H<sub>2</sub> in air. Table 2 lists the estimated parameters from the experimental response curves in Figure 4. The catalyst of the TGS device was heated up to 120 °C by its micro-heater with a heater power of 50.0 mW.

**Figure 3.** The flow rate dependence of the time constant,  $\tau$ , and the voltage difference,  $\Delta V_{\text{gas}}$ , at the TGS for 200 ppm  $\text{H}_2$  in air and the flow rate from 200 ccm to 1,800 ccm.



**Figure 4.** Experimental response curve of the TGS in the gas at a flow rate of 1,800 ccm of 200 ppm and 1,000 ppm  $\text{H}_2$  in air. The catalyst of the TGS device was heated up to 120 °C by its micro-heater.  $\text{H}_2$  flow was from 30 to 60 s. The thermal time constant  $\tau_A$ , measured as the elapsed time from 60 s to decreasing at 63.2% of the  $\Delta V_{\text{gas}}$  is 2.0 s.



Assuming that the thickness of Pt heater pattern on the TGS is constant,  $Q_{\text{heaterA}}$  and  $Q_{\text{heaterB}}$  were designed to be the same and were estimated to be 10.0 mW from the dimensions of the Pt heater pattern measured by the optical microscope image and Joule's laws. As shown in Figure 4, the thermal time constants of two signal curves were the same and equal to 8 s. The gas flow was introduced at steady state after the micro-heater had stabilized. We can then regard the time constant of 2.0 s as  $\tau_A$ , as described in Equation (15). From  $C_A$  in Table 1 and the thermal time constant of section A,  $\tau_A = R_A \times C_A$ ,  $R_A$  was estimated to be 230.4 K/mW. Using this value for  $\tau_A$  and  $V_{\text{air}} = -0.435$  mV in Figure 4,  $R_B$  was estimated as 230.6 K/mW, and  $\tau_B$  was calculated as 1 s.  $Q_{\text{catalyst}}$  can be calculated from Equation (10) as follows:

$$Q_{\text{catalyst}} = \frac{\Delta V_{\text{gas}}}{\alpha \times R_A} = 0.0217 \text{ [W/V]} \times \Delta V_{\text{gas}} \quad (16)$$

$Q_{catalyst}$  required for 1 mV of  $\Delta V_{gas}$  was calculated to be 21.7  $\mu$ W. The reciprocal of the coefficient of 46.1 in Equation (16) is a parameter representing voltage per unit catalytic combustion heat [V/W] that represents the efficiency of the TGS device.  $\Delta V_{gas}$  of the TGS for 200 and 1,000 ppm H<sub>2</sub> was 0.170 and 0.537 mV, respectively, and the expected  $Q_{catalyst}$  using Equation (16) for 200 and 1,000 ppm H<sub>2</sub> was estimated as 3.69  $\mu$ W and 11.7  $\mu$ W, respectively. An enthalpy of hydrogen combustion is 286 kJ/mol. The molar quantity of hydrogen combustion of TGS is  $3.35 \times 10^{-6}$  mol/s since the heat generation of 1,000 ppm hydrogen combustion is 11.7  $\mu$ W.

**Table 2.** Estimated parameters from the experimental response curve of the TGS for 200 ppm and 1,000 ppm hydrogen (Figure 4). The catalyst of the TGS device was heated up to 120 °C by its micro-heater.

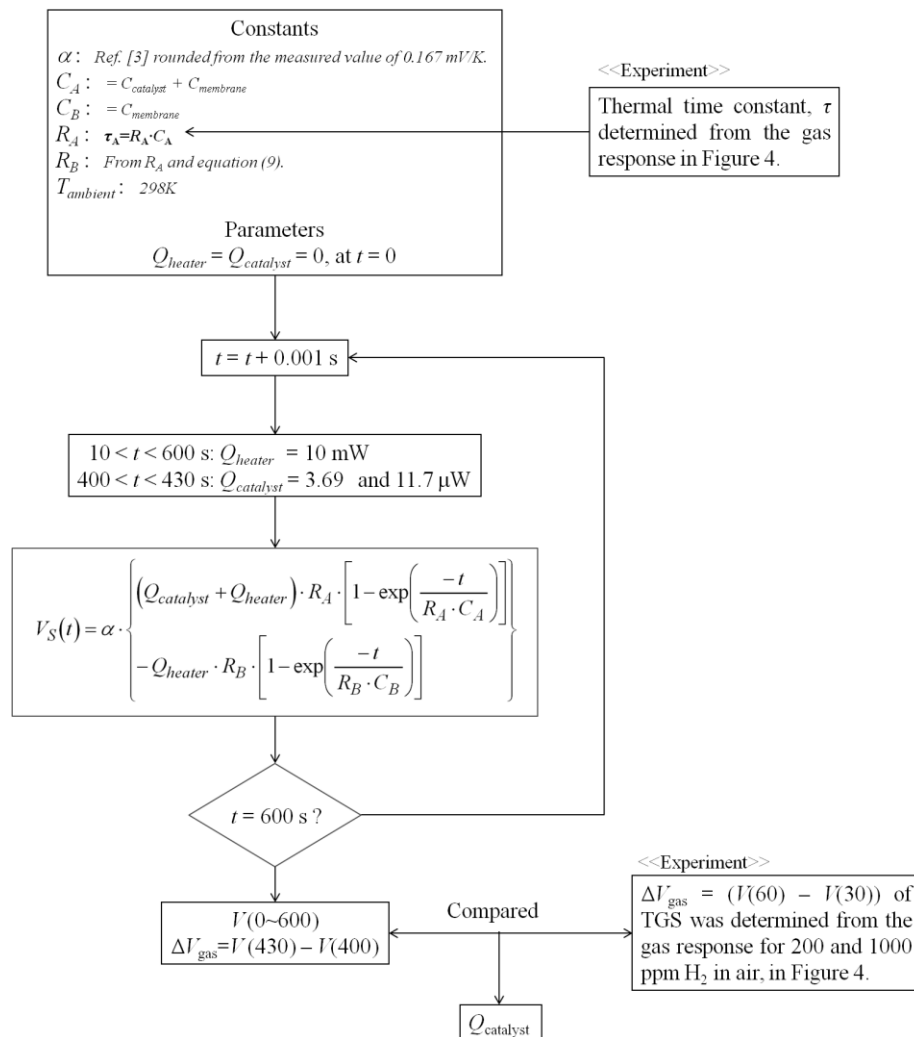
Parameter	Symbol	Value	Unit	Reference
Voltage signal of the TGS in air	$V_{air}$	-0.435	mV	Measured, Assuming that the thickness of Pt heater pattern on the TGS is constant, $Q_{heaterA}$ and $Q_{heaterB}$ were designed to be the same and were estimated to be 10.0 mW from the dimensions of the Pt heater pattern measured by the optical microscope image and Joule's laws. As shown in Figure 4, the thermal time constants of two signal curves were the same and equal to 8 s. The gas flow was introduced at steady state after the micro-heater had stabilized. We can then regard the time constant of 2.0 s as $\tau_A$ , as described in Equation (15). From $C_A$ in Table 1 and the thermal time constant of section A, $\tau_A = R_A \times C_A$ , $R_A$ was estimated to be 230.4 K/mW. Using this value for $\tau_A$ and $V_{air} = -0.435$ mV in Figure 4, $R_B$ was estimated as 230.6 K/mW, and $\tau_B$ was calculated as 1 s. $Q_{catalyst}$ can be calculated from Equation (16) as follows: $Q_{catalyst} = \frac{\Delta V_{gas}}{\alpha \cdot R_A} = 0.0217 [W/V] \times \Delta V_{gas}$
Whole heater power 50 mW	-	50.0	mW	Measured and rounded
Heater power of sections A and B	$Q_{heaterA}$ $Q_{heaterB}$	10.0	mW	Estimated from each heater pattern size dimension and the whole heater power 50 mW
Time constant of section A	$\tau_A$	2.0	s	Estimated from gas response of the TGS, Figure 4
Time constant of section B	$\tau_B$	1.0	s	From $\tau_B = R_B \times C_B$ , Equation (14)
Thermal resistance of section A	$R_A$	230.4	K/mW	From $\tau_A = R_A \times C_A$ , Equation (13)
Thermal resistance of section B	$R_B$	230.6	K/mW	From $V_{air} = \alpha \times Q_{heater} \times (R_A - R_B)$ , Equation (9)

\* The elapsed time at 63.2% of the saturated  $\Delta V_{gas}$ .

#### 4.4. Simulated Voltage Signal Response $V_S(t)$

Simulations were performed using Equation (15). The flow scheme of the simulation is shown in Figure 5. The simulation time was 600 s, where the heater operation was carried out after 10 s, assuming that the catalyst generates heat from 400 to 430 s. The simulation time step was 1 ms. Figure 6 shows the simulated response curves for  $V_S$  of the TGS as a function of  $Q_{catalyst}$  from 5.0 to 15.0  $\mu\text{W}$ .  $\Delta V_{gas}$  of the TGS for  $Q_{catalyst} = 3.69$  and 11.7  $\mu\text{W}$  was 0.230, 0.460, and 0.691 mV, respectively.

**Figure 5.** Flow chart for the simulation for calculating the voltage signal  $V_S(t)$  in Equation (15) of TGS compared to the experimental response  $\Delta V_{gas}$  of TGS.



The signal curves in Figure 6 match the signals in Figure 4. However,  $\Delta V_{gas}$  of the 1,000 ppm hydrogen in Figure 4 increased slightly with increasing time. Because  $Q_{catalyst}$  increased with increasing catalytic activity since the catalyst temperature increased with the 1,000 ppm  $\text{H}_2$  combustion. In Figure 6, the voltage signal was saturated since  $Q_{catalyst}$  was constant. In case of the voltage signal of the 200 ppm hydrogen in Figure 2, the catalytic activity was stable since the voltage signal was saturated. It is easy to calculate the voltage signal of TGS with the combustion of the low  $\text{H}_2$ .

$R_A$  in this study has been calculated from the time constant of 2 s. Comparing this to the value 0.05 s of our previous report [11], then the new  $R_A$  is estimated to be 5.8 K/mW. The reason why the  $R_A$  is too large is due to the fact the gas combustion process requires a thermally induced slow reaction and this makes the time constant much longer, which leads to a huge apparent thermal resistance. It is originated from the DELAYED time constant problem, which is very unique and a difficult problem of the chemical reaction of catalytic combustion.

One important parameter of the gas sensor device is how fast the sensor responds to the gas, *i.e.*, the time constant. We have investigated the effect of the heat capacity of the catalyst thickness  $d_{catalyst}$  on the thermal time constant, as shown in Figure 7.

**Figure 6.** The simulated response curves for  $\Delta V_{gas}$  of the TGS for  $Q_{catalyst} = 3.7$  and  $11.7 \mu W$  which correspond to 200 and 1,000 ppm  $H_2$  detection (Figure 4). The other parameters are unchanged and listed in Tables 1 and 2. The simulation results are from 380 to 460 s.  $Q_{catalyst}$  is nonzero from 400 s to 430 s.

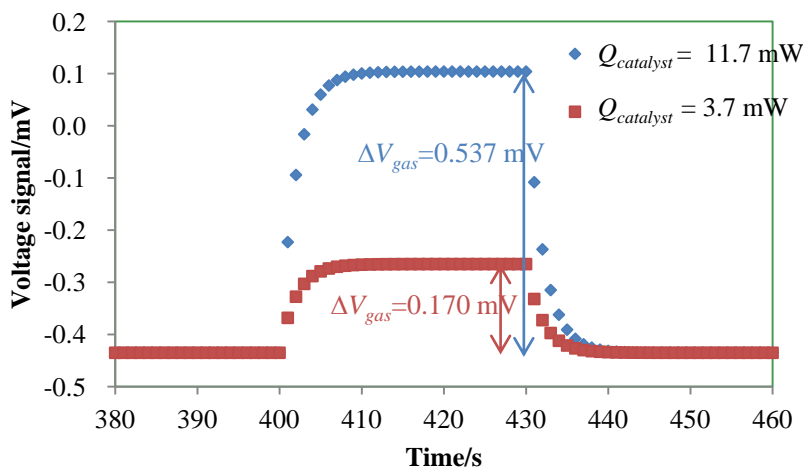
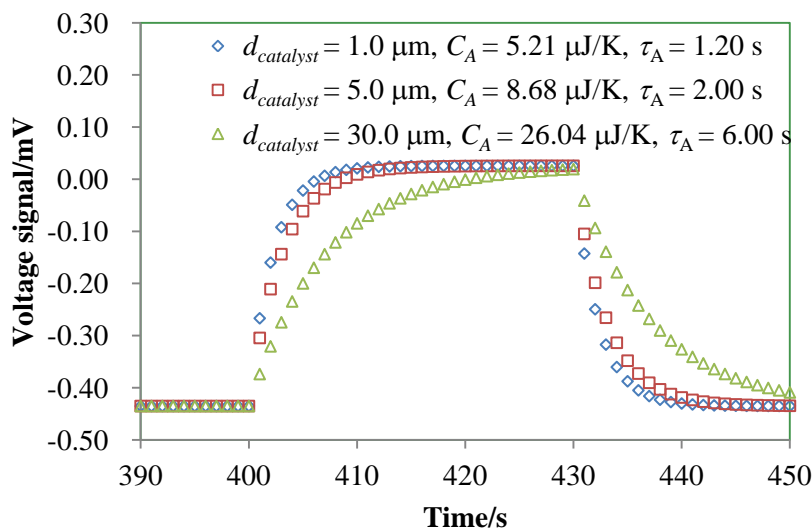


**Figure 7.** Simulated response curve of the TGS as a function of the catalyst thickness  $d_{catalyst}$ . The catalytic combustion heat  $Q_{catalyst}$  was  $10.0 \mu W$ .



In our TGS device, a performance enhancement can be achieved by reducing  $d_{catalyst}$ . The increase in the time constant with an increase in the dimension of the catalyst has also been plotted as a

function of  $d_{catalyst}$  from 1.00 to 30.0  $\mu\text{m}$ . The values of  $\tau_A$  for  $d_{catalyst} = 1.00, 5.00, \text{ and } 30.0 \mu\text{m}$  were 1.2, 2.0 and 6.0 s, respectively.  $Q_{catalyst}$  required for 1.0 mV of  $\Delta V_{gas}$  was calculated to be 0.0217 mW.  $\tau_H$  is 2 s and  $\tau_A$  is 0.1 s.  $\tau_H$  is bigger than  $\tau_A$  since the supply rate of  $\text{H}_2$  limits the rate of the combustion for  $\text{H}_2$ .

## 5. Conclusions

We have analyzed the thermal balance of a micro-TGS, calculated the heat balance at the two sections across a TE film of the TGS device, and estimated the sensor output voltage.  $R_A$  and  $R_B$  at the two sections were estimated to be 230.4 K/mW and 230.6 K/mW from the thermal time constants of the experimental signal curves.  $Q_{catalyst}$  required for 1 mV of  $\Delta V_{gas}$  was calculated to be 0.0217 mW. On the basis of these parameters, simulations for the device performance were performed, and the expected  $Q_{catalyst}$  for 200 and 1,000 ppm  $\text{H}_2$  was 3.69  $\mu\text{W}$  and 11.7  $\mu\text{W}$ , respectively.

## Acknowledgments

This work was supported by the project entitled “Development Project for Extremely-Early Diagnostics Technologies for Human Diseases” of Aichi Prefecture, Japan.

## Conflicts of Interest

The authors declare no conflict of interest.

## References

1. Behall, K.M.; Scholfield, D.J.; van der Sluijs, A.M.; Hallfrisch, J. Breath hydrogen and methane expiration in men and women after oat extract consumption. *J. Nutr.* **1998**, *128*, 79–84.
2. Roberge, M.T.; Finley, J.W.; Lukaski, H.C.; Borgerding, A.J. Evaluation of the pulsed discharge helium ionization detector for the analysis of hydrogen and methane in breath. *J. Chromatogr. A* **2004**, *1027*, 19–23.
3. Nishibori, M.; Shin, W.; Houlet, L.F.; Tajima, K.; Itoh, T.; Murayama, N.; Matsubara, I. New structural design of micro-thermoelectric sensor for wide range hydrogen detection. *J. Ceram. Soc. Jpn.* **2006**, *114*, 853–856.
4. Shin, W.; Nishibori, M.; Izu, N.; Itoh, T.; Matsubara, I.; Nose, K.; Shimouchi, A. Monitoring breath hydrogen using thermoelectric sensor. *Sens. Lett.* **2011**, *9*, 684–687.
5. Shin, W.; Nishibori, M.; Houlet, L.F.; Itoh, T.; Izu, N.; Matsubara, I. Fabrication of thermoelectric gas sensors on micro-hotplates. *Sens. Actuators B Chem.* **2009**, *139*, 340–345.
6. Wagman, D.D.; Evans, W.H.; Parker, V.B.; Schumm, R.H.; Halow, I.; Balley, S.M.; Churney, K.L.; Nuttall, R.L. *The NBS Tables of Chemical Thermodynamic Properties. Selected Values for Inorganic and C1 and C2 Organic Substances in SI Units*; American Chemical Society: Washington, DC, USA, 1982.
7. Zumdahl, S.S.; Zumdahl, S.L.; Decoste, D.J. *World of Chemistry*; Houghton Mifflin Company: Boston, MA, USA, 2002.

8. van Oudheusden, B.W. Effect of operating conditions on the dynamic response of thermal sensors with and without analog feedback. *Sens. Actuators A Phys.* **1997**, *58*, 129–135.
9. Simon, I.; Barsan, N.; Bauer, M.; Weimar, U. Micromachined metal oxide gas sensors: opportunities to improve sensor performance. *Sens. Actuators B Chem.* **2001**, *73*, 1–26.
10. Gospel, W.; Hesse, J.; Zemel, J.N. *Sensors A Comprehensive Survey*; WILEY VCH: Weinheim, Germany, 1990; pp. 11–69.
11. Houlet, L.F.; Tajima, K.; Shin, W.; Itoh, T.; Izu, N.; Matsubara, I. Platinum micro-hotplates on thermal insulated structure for micro-thermoelectric gas sensor. *IEE J Trans. Sens. Micromach.* **2006**, *126*, 568–572.

© 2014 by the authors; licensee MDPI, Basel, Switzerland. This article is an open access article distributed under the terms and conditions of the Creative Commons Attribution license (<http://creativecommons.org/licenses/by/3.0/>).